JOURNAL OF PROPULSION AND POWER
Vol. 15, No. 2, March–April 1999

Technical Notes

TECHNICAL NOTES are short manuscripts describing new developments or important results of a preliminary nature. These Notes cannot exceed 6 manuscript pages and 3 figures; a page of text may be substituted for a figure and vice versa. After informal review by the editors, they may be published within a few months of the date of receipt. Style requirements are the same as for regular contributions (see inside back cover).

Advanced Mixing Control in Supersonic Airstream with a Wall-Mounted Cavity

N. Sato,* A. Imamura,* S. Shiba,* S. Takahashi,†
M. Tsue,‡ and M. Kono§
University of Tokyo, Tokyo 113, Japan

Nomenclature

D = cavity depth
L = cavity length
M_c = convective Mach number
U = velocity
ρ = density

Subscripts
1 = main airflow
2 = injected gas flow

Introduction

MIXING between supersonic air and gaseous fuel dominates the combustion process in a scramjet engine combustor. However, the growth rate of the mixing layer decreases as the convective Mach number increases, owing to compressibility effects.[1] Several methods to enhance and control the mixing have been studied. Streamwise vortex generated by the ramps in the supersonic airstream was proven to be effective for mixing enhancement.[2] On the other hand, two-dimensional instability that causes large-scale rollers is expected to be effective for the mixing.[3] However, at higher Mach numbers, it is known that the two-dimensional instability is suppressed. The authors noticed that the acoustic feedback of the underexpanded jet led to its oscillation,[4] and assumed that the two-dimensional instability enhancement might be possible if a strong acoustic wave impinged on the initial condition of the supersonic mixing layer. The cavity was thought to be one of the best acoustic drivers to generate acoustic waves strong enough to disturb the stable supersonic flow. Yu and Schadow[5] also used a cavity to enhance the mixing of supersonic nonreacting jets.

Presented as Paper 96-4510 at the AIAA 7th International Space Planes and Hypersonic Systems and Technologies Conference, Norfolk, VA, Nov. 18–22, 1996; received April 28, 1997; revision received Sept. 6, 1998; accepted for publication Sept. 14, 1998.

*Graduate Student, Department of Aeronautics and Astronautics, Faculty of Engineering, 7-3-1 Hongo, Bunkyo-ku. E-mail: naohiro@jamss.co.jp.

†Research Associate, Department of Aeronautics and Astronautics, Faculty of Engineering, 7-3-1 Hongo, Bunkyo-ku.

‡Associate Professor, Department of Aeronautics and Astronautics, Faculty of Engineering, 7-3-1 Hongo, Bunkyo-ku.

§Professor, Department of Aeronautics and Astronautics, Faculty of Engineering, 7-3-1 Hongo, Bunkyo-ku.

In this Note, it is reported how the acoustic wave impinging on the initial condition of the supersonic mixing layer affected its growth.

Experimental Setup

The schematic of the flow at the two-dimensional nozzle exit is shown in Fig. 1, with the axes whose origin was set on the center of the injector exit. The width was 46 mm. An extended strut was installed on the centerline of the nozzle upstream of the throat to make shock-free conditions. The secondary air was injected behind the strut. The height of the injector exit was 3 mm, and its width was same with that of the nozzle exit, 46 mm. The nozzle sidewalls extended 60 mm downstream from the nozzle exit. For flow visualization, optical glasses were installed into the walls. The main airflow Mach number was 1.78, and the velocity was 474 m/s. The total temperature was 288 K, and the exit static pressure was atmospheric. The Reynolds number was 2.23×10^5, based on the extended strut height $H = 4$ mm.

The cavity was located upstream of the nozzle exit. The acoustic waves generated by the cavity impinged near the rear of the strut, as shown in Fig. 1. A typical schlieren image of the cavity exit is also shown. The technique is described next. In the schlieren image, the sidewall was replaced and the cavity was set at the nozzle exit to visualize the flow around the cavity exit.

Table 1 shows the experimental conditions. The secondary air injection conditions from case 1 to case 3 are the same. Subsonic air was injected parallel to the main airstream, and two cavity shapes were tested.

Mean pitot pressure was measured with 0.6-mm-o.d. and 0.4-mm-i.d. pitot probes set on a Y-traverse stage, moved every 0.5 mm by a stepping motor. Schlieren photography was used to visualize the flow. An Xe flash lamp was used as the light source; the spark duration of the lamp was ~1 μs. The images

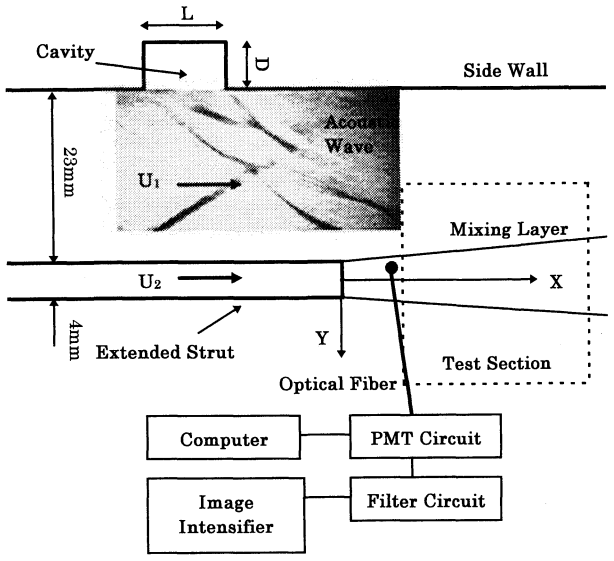

Fig. 1 Schematic of the flow at the nozzle exit.

Table 1 Experimental conditions

Case	Gas_2	U_2/U_1	ρ_2/ρ_1	M_c	Cavity shape, mm	Frequency, kHz
1	Air	0.21	0.61	0.62	——	——
2	Air	0.21	0.61	0.62	$L = 10$ $D = 5$	25
3	Air	0.21	0.61	0.62	$L = 10$ $L = 14$	38

were taken with a charge-coupled device camera. The direction of the knife edge was set parallel to the flow. The optical deflectmetry, similar to the quantitative schlieren technique of McIntyre and Settles,[6] was used to obtain fluctuation data of the acoustic wave and mixing layer. In the present experiment, a shadowgraph technique was used instead of a schlieren technique. A screen with a 0.5-mm-diam pinhole was set on the traverse stage. The diagram of the optical deflectometry system is also shown in Fig. 1. In this method, the fluctuations of the beam intensity integrated along the spanwise direction are proportional to those of the second derivative of the density. The peak heights of fundamental and subharmonic frequencies were uncertain because the beam intensity was very dependent on the density profile, so that it was difficult to know exactly what these heights were in the present experiment. This method was used to obtain a fundamental frequency of the fluctuation and synchronized images with the disturbance. The gate duration of the image intensifier was 1 μs. Ten to thirty instantaneous synchronized images were averaged. The measurement technique mentioned in the preceding text was adequate for a qualitative evaluation of the result.

Results and Discussion

A schlieren image without the disturbance is shown in Fig. 2a, with the range of the visualization. Near the injector exit, an expansion fan followed by a recompression wave is observed. Although small-scale turbulence is difficult to observe in the image, it is assumed to have been formed much like the result of the study by Clemens and Mungal.[7] The oscillation of the mixing layer starting near the injector exit was observed when the acoustic wave was impinged. An instantaneous schlieren image and a synchronized shadowgraph image in the case of $L = 10$ and $D = 14$ are shown in Figs. 2b and 2c. The signal of the optical deflectmetry for synchronizing the images was obtained around the upper side of the injector exit. With the disturbance, the mixing layer became unstable and oscillation occurred. Because nearly the same oscillation of the mixing layer can be observed in the synchronized image along with the instantaneous one, it can be concluded that the oscillation was caused by the disturbance. When the fluctuations of the beam intensity passing through the mixing layer were detected downstream, nearly the same fundamental frequency with the acoustic disturbance shown in Table 1 was obtained.

The pitot pressure profiles measured at $X/H = 5$, 7.5, and 10, along the X axis, are shown in Fig. 3. In every case, the momentum of the secondary air was smaller than that of the main flow. Thus, the pitot pressure in the mixing layer increases as the mixing continues. With the disturbance, the profiles expand toward the Y direction, and the minimum pitot pressures around $Y = 0$ increase. Figure 4 shows that the growth rates of the pitot pressure thickness defined in Fig. 3 become much larger because of the disturbance. The large growth rate of the mixing layer was thought to be a result of the mixing-layer oscillation shown in Fig. 2.

Because of data number limitations of the experiment and technique, the use of this result should be limited to qualitative evaluation. However, the phenomena explained in this report was proved to be reliable enough to show the possibility of enhancing two-dimensional structure evolution by the acoustic disturbance.

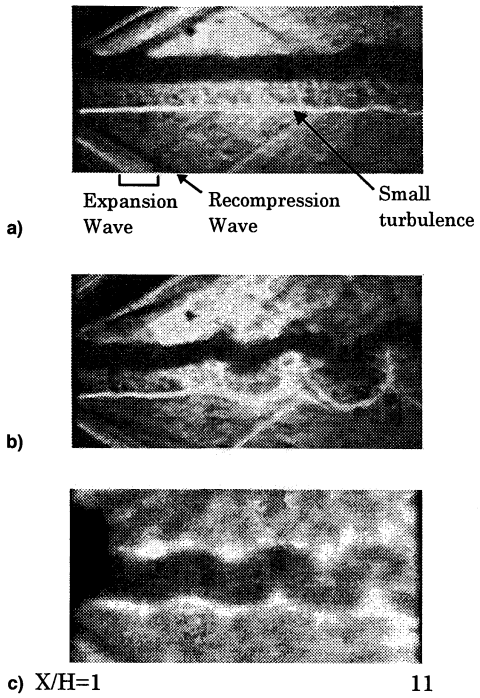

Fig. 2 Schlieren and shadowgraph images: a) schlieren image of case 1, b) schlieren image of case 3, and c) synchronized shadowgraph image of case 3.

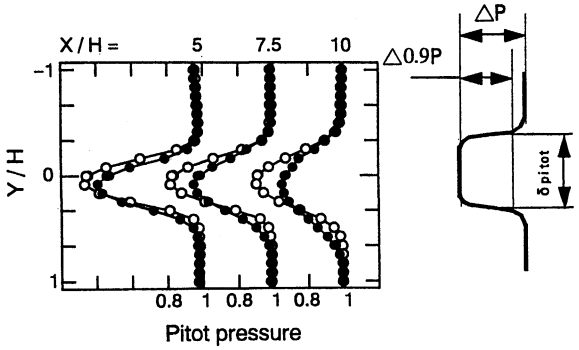

Fig. 3 Pitot pressure profiles. ○, without disturbance; ●, $L = 10$ and $D = 5$.

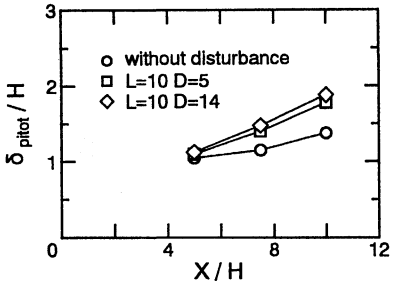

Fig. 4 Growth of the pitot pressure thickness.

Acknowledgments

The authors would like to thank H. Shimano, K. Okai, M. Utsumi, H. Itoh, K. Yamaguchi, S. Momo, and T. Iwata for their kind advice and help.

References

[1]Papamoschou, D., and Roshko, A., "The Compressible Turbulent Shear Layer: An Experimental Study," *Journal of Fluid Mechanics*, Vol. 197, Dec. 1988, pp. 453–477.

[2]Northam, G. B., Greenberg, I., and Byington, C. S., "An Investigation of Wall Injectors for Supersonic Mixing Enhancement," AIAA Paper 89-2525, July 1994.

[3]Buckmaster, J., Jackson, T. L., and Kumar, A., *Combustion in High-Speed Flows*, Kluwer Academic, Norwell, MA, 1994, pp. 131–190.

[4]Hammitt, A. G., "The Oscillation and Noise of an Overpressure Sonic Jet," *Journal of the Aerospace Science*, Vol. 28, No. 9, 1961, pp. 673–680.

[5]Yu, K. H., and Schadow, K. C., "Cavity-Actuated Supersonic Mixing and Combustion Control," *Combustion and Flame*, Vol. 99, No. 2, 1994, pp. 295–301.

[6]McIntyre, S. S., and Settles, G. S., "Optical Experiments on Axisymmetric Compressible Turbulent Mixing Layers," AIAA Paper 91-0623, Jan. 1991.

[7]Clemens, N. T., and Mungal, M. G., "Two- and Three-Dimensional Effects in the Supersonic Mixing Layer," *AIAA Journal*, Vol. 30, No. 4, 1992, pp. 973–981.

Formulation of Navier–Stokes Equations for Moving Grid and Boundary

Homayun K. Navaz* and Raymond M. Berg†
Kettering University, Flint, Michigan 48504-4898

Nomenclature

E = total energy
$\boldsymbol{E}, \boldsymbol{F}$ = flux vectors
f = force per unit mass
$\boldsymbol{G}$ = source term vector
H = total enthalpy
J = Jacobian of the transformation
n = 0 for two-dimensional flows, 1 for axisymmetric flows
P = pressure
$\boldsymbol{Q}$ = primitive variable vector
q = heat flux
r = radial direction
T = temperature
t = time
$\boldsymbol{U}$ = conserved variable vector
u, v = components of velocity in x and r directions
W = boundary work per unit mass of the fluid
x = axial direction
γ = specific heat ratio
μ = molecular viscosity
$\xi, \eta, \tilde{t}$ = computational coordinates
ρ = density
τ = shear stress tensor

Subscripts
r = refers to the radial direction
v = viscous flux
x = refers to the axial direction

Superscripts
T = transpose of a matrix
$\cdot$ = rate, change in time
$\sim$ = transformed coordinates

Received March 27, 1998; revision received Aug. 12, 1998; accepted for publication Aug. 20, 1998.

*Assistant Professor, Department of Mechanical Engineering, 1700 West Third Avenue.

†Lecturer, Department of Mechanical Engineering, 1700 West Third Avenue.

Introduction

In problems where a boundary is moving, part of the control volume energy can be consumed to displace the boundary, e.g., expansion, or the boundary can be utilized to increase the energy content of the control volume, e.g., compression. This effect can be included in the energy equation through a source term. The energy equation in the Navier–Stokes formulation contains the rate of work generated by the flow, and it does not include other types of energy that may influence the control volume such as the boundary work, shaft work, etc. Generally, the computational fluid dynamics (CFD) codes have mostly been applied to open systems with only the flow work being present in the formulation. There are several commercially available programs that are applied to closed systems such as the gun-barrel propulsion and internal combustion (IC) engines. However, these CFD codes with all degrees of sophistication must be able to reproduce good results for simple classic problems.

The transformation of the Navier–Stokes equations into a computational coordinate system is widely practiced in finite difference and finite volume methods.[1,2] This coordinate mapping introduces the transformation Jacobian J, a representation of a cell volume, into the equations. For a time-varying grid, the value of the Jacobian that is calculated for the purpose of evaluating the flow variables must be consistent with the value of the appropriate differential volume element; therefore, requiring a time derivative of the Jacobian to be included in the finite difference form of equations. This time derivative is part of the geometric conservation law (GCL). Thomas and Lombard[3] derived a geometric conservation law having the same integral form as the mass conservation. Gaitonde and Fiddes[4] applied the GCL to the finite volume solution of the Navier–Stokes equation. To the best of our knowledge, the requirements for an energy source/sink term and time derivative of the transformation Jacobian are sometimes ignored by CFD practitioners.

In this paper, we examine the effects of the inconsistency in the computation of the effective volume element associated with moving grids, and the boundary work on the solution of conservation equations, for a simple isentropic expansion problem of a closed system. The liquid thrust chamber performance (LTCP) code,[5] which is based on finite difference discretization with a total variation diminishing (TVD) scheme, with options to be applied to Lax–Friedrichs, Van–Leer, or Roe numerical fluxes, is used as a vehicle for this study.

Theory

The Navier–Stokes equations for compressible flow of gases in a two-dimensional/axisymmetric coordinate system are

$$\frac{\partial \boldsymbol{U}}{\partial t} + \frac{\partial \boldsymbol{E}}{\partial x} + \frac{\partial \boldsymbol{E}_v}{\partial x} + \frac{\partial \boldsymbol{F}}{\partial r} + \frac{\partial \boldsymbol{F}_v}{\partial r} + \boldsymbol{G} = 0 \tag{1}$$

where $\boldsymbol{U}$ is the conserved variable vector, $\boldsymbol{E}$ and $\boldsymbol{F}$ are the two components of inviscid flux vectors and $\boldsymbol{E}_v$ and $\boldsymbol{F}_v$ are their viscous counterparts, and $\boldsymbol{G}$ is the source term. These terms are, respectively, defined as

$$\boldsymbol{U} = r^n(\rho u, \rho v, E, \rho)^T \tag{2a}$$

$$\boldsymbol{E} = r^n(\rho u^2 + P, \rho uv, \rho uH, \rho u)^T \tag{2b}$$